Saturation analysis as a test of statistical fission in heavy ion reactions

M. Blann, D. Akers, T. A. Komoto, F. S. Dietrich, L. F. Hansen, and J. G. Woodworth
E-Division, Lawrence Livermore National Laboratory, Livermore, California 94550

W. Scobel
I. Institut für Experimental Physik, University of Hamburg, Hamburg, Federal Republic of Germany

J. Bisplinghoff
Institut für Strahlen und Kemphysik, Bonn University, Bonn, Federal Republic of Germany

B. Sikora
The Institute of Experimental Physics, Department of Nuclear Physics, Warsaw University, Warsaw, Poland

F. Plasil and R. L. Ferguson
Physics Division, Oak Ridge National Laboratory, Oak Ridge, Tennessee 37830
(Received 27 May 1982)

Evaporation residue and binary (fissionlike) cross sections are reported for $^{56}Fe+^{120,122}Sn$ at incident ^{56}Fe energies between 330 and 456 MeV. The σ_{ER} are compared with results for the two additional entrance channels $^{35}Cl+^{141}Pr$ and $^{86}Kr+^{90}Zr$ producing similar compound nuclei. Comparisons of $\sigma_{ER}/\pi\lambda\!\!\!^{-2}$ versus excitation energy (which tests the Bohr independence hypothesis) support the conclusion that the yields are limited by statistical fission decay. Similar results are shown for the entrance channels $^{84,86}Kr+^{65}Cu$ and $^{40}Ar+^{109}Ag$. It is shown that evaporation residue data of this type (where yields are limited by saturation in the fission channel) provide a good means of determining statistical fission parameters.

[NUCLEAR REACTIONS Illustrate consistency of evaporation residue excitation functions formed in heavy ion reactions with Bohr independence hypothesis; illustrate that statistical parameters deduced should be valid.]

I. INTRODUCTION

Many experiments have been performed where fission and evaporation residue (ER) excitation functions are measured both for the purpose of deducing statistical model fission parameters and/or fusion barrier parameters.[1-8] Emphasis on the statistical fitting process is often placed on the fission threshold region of the excitation functions where the fission cross sections σ_f are much lower than the evaporation residue cross sections σ_{ER}. Indeed, in some cases there is a reticence to accept analyses of data for which the binary division cross section is large because it is suspected that there may be contributions of noncompound cross sections.

In this work, we expand upon the suggestion[9,10] that analyses of data in the region $\sigma_f \gg \sigma_{ER}$ should not only give valid statistical parameters, but indeed offer some distinct advantages and possibly fewer ambiguities than for the case $\sigma_f \ll \sigma_{ER}$. Indeed the subsequent discussion will show that each region simultaneously offers advantages and disadvantages, and that the two regions are in a sense complementary. The $\sigma_f \gg \sigma_{ER}$ data are valuable when the limit to high J partial waves contributing to ER formation results completely from the competition of equilibrium fission. If this condition is fulfilled, our thesis is that contamination of the binary division cross section by other than equilibrium fission components will not alter the parameters deduced by fitting the ER excitation functions. Because this analysis requires that some partial waves above the ER survival limits go entirely into equilibrium fission (i.e., are saturated by fission deexcitation), we will refer to this approach as "saturation analysis." The data must therefore lie in a region where the evaporation residue cross sections are no longer increasing in approximate proportion to the reaction cross section. If the saturation condition is

fulfilled, then measured $\sigma_{ER}/\pi\lambda\!\!\!^{-2}$ (where $\lambda\!\!\!^{-}$ is the reduced de Broglie wavelength in the entrance channel) for different entrance channels leading to the same composite nuclei should all fall on a single curve when plotted versus excitation energy. This is a consequence of the Bohr independence hypothesis. Such a comparison of experimental results provides a model independent test as to whether or not the σ_{ER} resulting from different entrance channels are mutually consistent with an equilibrium formation mechanism. We will expand upon these statements in Sec. II.

Motivated by the reasons given above, we have measured ER (and binary decay) excitation functions for the reactions $^{56}Fe+^{120,122}Sn$, and compared them with published results[3,9–11] for the reactions $^{35}Cl+^{141}Pr$ and $^{86}Kr+^{90}Zr$. These systems make $^{176,178}Os$ compound nuclei. Experimental results are presented in Sec. III. In Sec. IV, we will show that comparisons of data from the three entrance channels producing Os composite nuclei, and of data for two channels producing Tb nuclei, do support the saturation requirement and the Bohr independence hypothesis. In Sec. V, statistical model comparisons are presented for these data sets, in order to illustrate that fits to saturation data are indeed quite sensitive to the choice of statistical fission parameters; however, no attempt is made to extract best parameter sets. In Sec. VI, we present discussion and conclusions, with suggestions for future work desirable in this area.

II. REQUIRED CONDITIONS FOR THE VALIDITY OF SATURATION ANALYSIS

The conditions required for saturation analysis to be valid are illustrated in Fig. 1, which is intended to show a possible qualitative scenario for divisions of partial entrance channel cross sections σ_J vs J. First, there should be some number of partial waves (e.g., 0 to J_3) in the entrance channel which go entirely into compound nucleus formation; all higher waves may go into any admixture of reaction channels. A major portion of compound nuclei in a range of angular momenta $J \geq J_2$ should undergo fission, along with some fraction of the partial waves in the region $J \geq J_1$. The dotted curve between J_1 and J_2 represents the region where increasing fractions of the higher J go into fission (the area above the dotted line) and decreasing fractions survive fission (the area below the line). The dotted curve between J_3 and J_4 represents a smooth cutoff

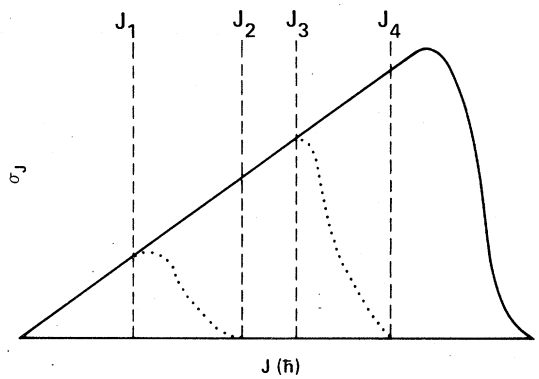

FIG. 1. Qualitative representation of the reaction cross section division which would be required for the saturation hypothesis of this work to be valid. The figure is discussed in Sec. II.

between compound and noncompound reactions. This is a reasonable qualitative description of division of partial waves when sufficiently high J are in the entrance channel, unless the ER cross section is limited not by equilibrium fission but in the entrance channel due to trajectories which do not pass inside the true saddle point. This seems a simple qualitative statement of *possible* divisions of entrance channel angular momenta.

If the saturation condition given above is met (the ER yields are limited totally by fission), then fitting the ER excitation function by a statistical fission model with parameter variation amounts to adjusting the parameters to give the demarcation zone shown in Fig. 1 between J_1 and J_2 for ER survival (or the weighted average J between J_1 and J_2 for ER products). The choice of these parameters is totally independent of contributions to the fissionlike cross section for $J > J_2$. However, we must address the question as to whether the ER survival results from equilibrium fission competition, or from an entrance channel effect. If the former, we would expect the distribution of partial waves surviving fission (the dashed curve between J_1 and J_2 in Fig. 1) to depend only on the excitation energy of the compound nucleus (the Bohr hypothesis). The reduced evaporation residue cross sections (RCS) given by $\sigma_{ER}/\pi\lambda\!\!\!^{-2}$ from any entrance channel to produce a given compound nucleus should fall on a single curve when plotted versus excitation energy (since the fraction of each partial wave J surviving fission should be independent of the mode of formation).

If, on the other hand, the σ_{ER} results from entrance channel limitations, and if the different entrance channels are expected to have considerably

different fusion trajectories, then one would not expect to obtain such a correlation of reduced ER excitation functions purely fortuitously. These comparisons are made in Sec. IV. First, we present results of σ_{ER} and fissionlike yield measurements for reactions of ^{56}Fe on ^{120,122}Sn, which are compared with published data for other entrance channels in Sec. IV.

III. EXPERIMENTAL PROCEDURES AND RESULTS

These experiments were performed using the Lawrence Berkeley Laboratory (LBL) Superhilac accelerator. Beams of ^{56}Fe at energies between 330 and 456 MeV were used on self-supporting targets of ^{120}Sn (220 μg/cm^2) and ^{122}Sn (167 μg/cm^2). The beam energies were determined using Si counters at 0° and phase probe measurements. Energies reported are thought to be accurate to ± 3 MeV.

The reaction products were detected using a telescope consisting of two microchannel plates (0.75 m apart) for flight time, an ion chamber for ionization, and an Si diode for energy determination. Data were recorded in event mode. Calibration of mass and charge algorithms was aided by a ^{84}Kr beam. This provided elastic and slit scattered spectra of ^{84}Kr, which along with the ^{56}Fe beam data allowed us to find calibration parameters which simultaneously gave both masses and charges correctly over a broad energy range.

The apparatus and experimental procedures are described in detail elsewhere.[11,12] The ER angular distributions are shown in Fig. 2; angle integrated cross sections are summarized in Table I.

Binary decay products were measured at angles of 8°, 10°, 20°, and 28°. Mass yields were summed in bins of 2 u width. Results for laboratory angles of 10° and 28° are shown in Figs. 3 and 4. Error bars typical of the counting statistics are shown on representative data points, which are given only relative values on the ordinate. Smooth curves were drawn through the experimental points, and these were converted to mb/u (c.m.); these results are shown by the dashed curves in Figs. 3 and 4. Results at 8° and 20° are similar as to quality of data.

Angular distributions for different masses were plotted as illustrated in Fig. 5 for the (typical) 350 MeV data. $\mathrm{Sin}\theta^{-1}$ curves were fitted through points of the type shown in Fig. 5, and these curves were integrated to give the cross section (σ_A) for each mass number (A). The curves of σ_A vs A were summed from an estimated symmetry mass to the high mass limit ($A \approx 130$) to give "fissionlike" yield cross sections. Because points at angles beyond 90° c.m. were not measured, we can only make the statement that the fragment angular distributions are not inconsistent with the expectations of equilibrium fission. However, as discussed in Sec. II, a saturation analysis does not require measurement of the fissionlike cross sections; consequently the lack of backward angle data is not important to the present approach, which is based solely on ER excitation function analyses.

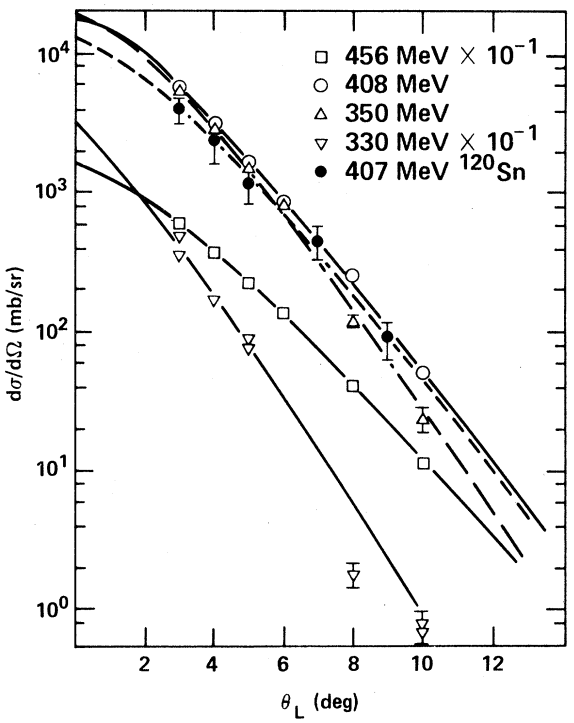

FIG. 2. Evaporation residue angular distributions.

IV. SATURATION COMPARISONS OF EXPERIMENTAL ER CROSS SECTIONS

In Sec. II, it was argued that *if* evaporation residue cross sections are limited by the survival of

TABLE I. Experimental results ^{56}Fe+Sn.

Beam energy (MeV lab)	Evaporation residue cross section (mb)	Fissionlike cross section (mb)	Target
330±3	155±40	1050±300	^{122}Sn
350±3	155±40	1150±300	^{122}Sn
408±3	165±40	1070±300	^{122}Sn
456±3	185±45	1030±300	^{122}Sn
407±3	130±40		^{120}Sn

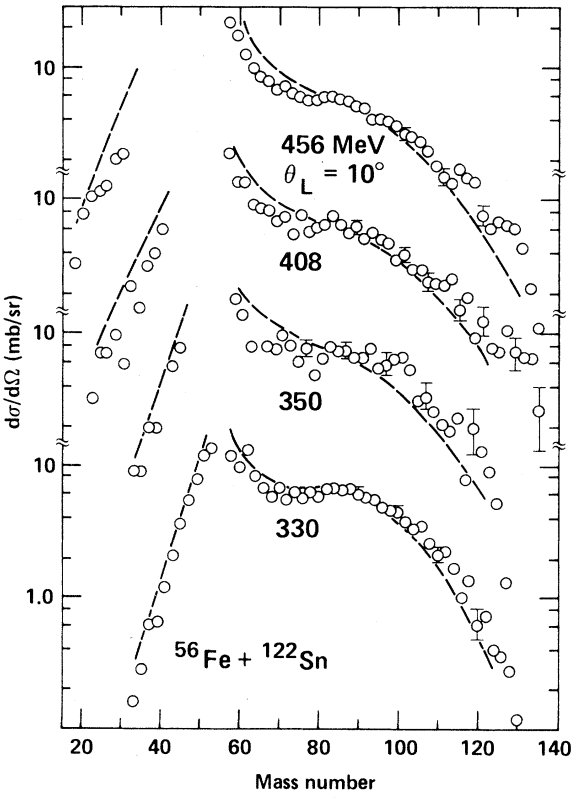

FIG. 3. Binary decay yields versus mass number at 10° (lab). Error bars on representative points indicate statistical errors only; the ordinate is relative for the experimental points. The dashed curves represent smooth curves drawn through the experimental points, transformed to cross sections per mass. The ordinate is in millibarns for the dashed curves.

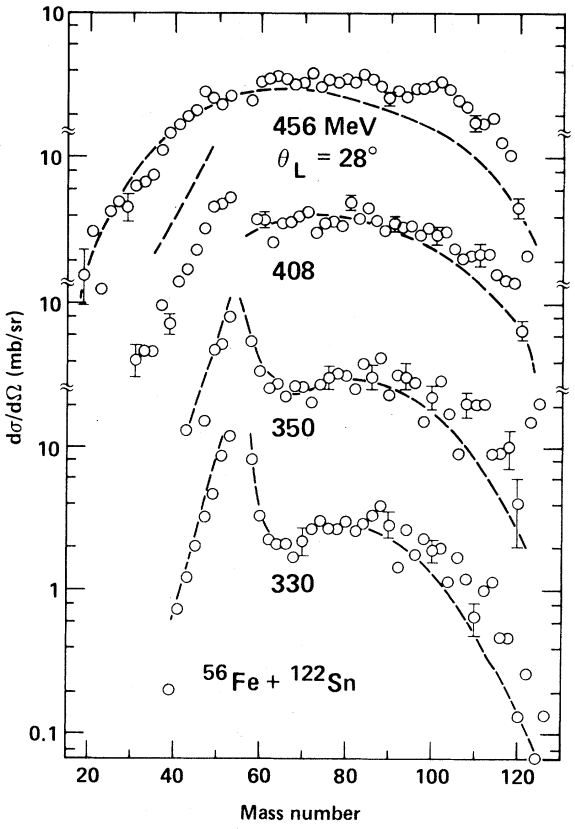

FIG. 4. As in Fig. 3 but at 28° (lab).

compound nucleus fission deexcitation of the higher partial waves, then according to the Bohr hypothesis, the relative population of partial waves surviving fission should depend only on the compound nucleus excitation energy. The evaporation residue cross sections must be presented as reduced cross sections in such a comparison, e.g., by dividing by $\pi\lambda\!\!\!^{-2}$ where $\lambda\!\!\!^{-}$ is the reduced de Broglie wavelength in the entrance channel. The reduced σ_{ER} are proportional to the sums over the fraction of partial waves surviving fission, where the sum extends to partial waves which have effectively zero fission survival, and where all reduced σ_{ER} have the same proportionality constant (due to division by $\pi\lambda\!\!\!^{-2}$).

We compare two systems, ^{176}Os and ^{149}Tb, in this work—accepting also, as equivalent, reactions leading to composite systems with two more neutrons, since fission survival at saturation should be similar within this tolerance. For the first system the results reported in Sec. III are compared with results from the reactions ^{86}Kr+^{90}Zr and ^{35}Cl+^{141}Pr using published cross sections.[1,3,10,11] Results for the ^{149}Tb system are based on the reactions ^{40}Ar+^{109}Ag and ^{84,86}Kr+^{65}Cu, also taken from the literature.[4]

Reduced cross sections for these systems are shown versus compound nucleus excitation energy in Figs. 6 and 7. The scales are quite expanded with respect to the estimated fusion cross sections. Perspective on this point is shown in Fig. 8, where the reduced fusion (fissionlike plus ER) cross sections are shown as well as the reduced ER cross sections for the Os system. Figures 6—8 show that the experimental points for each system all fall on a single curve to within the experimental uncertainties, with the exception of a few points which we will discuss. A straight line, in fact, provides a satisfactory fit to the data, although there is no *a priori* reason why this should be so. We have drawn arbitrary lines through the points in Figs. 6—8 just to illustrate the adequacy of a straight line fit; the

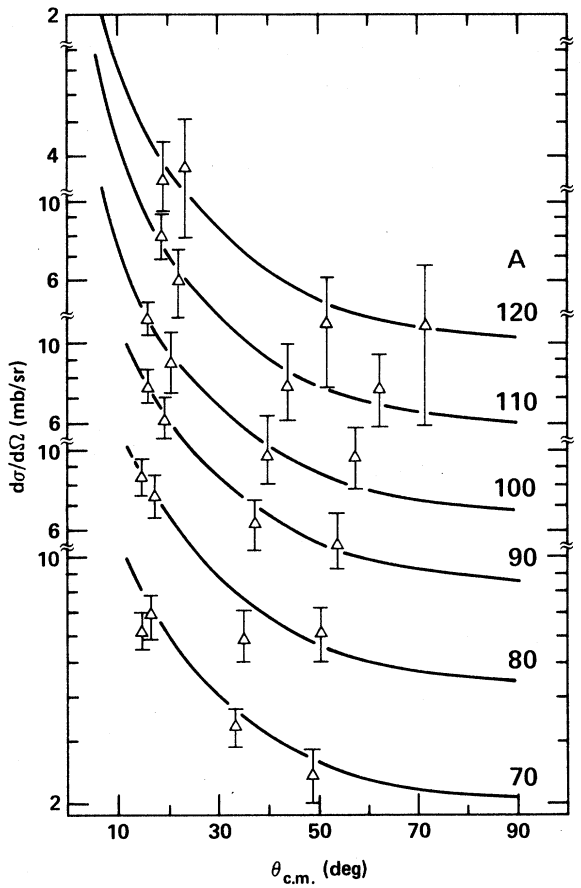

FIG. 5. Angular distributions (c.m.) for representative fissionlike masses at 350 MeV incident ^{56}Fe energy on ^{122}Sn targets. Curves of the form $\sin\theta^{-1}$ are indicated. These results are representative of the other energies measured.

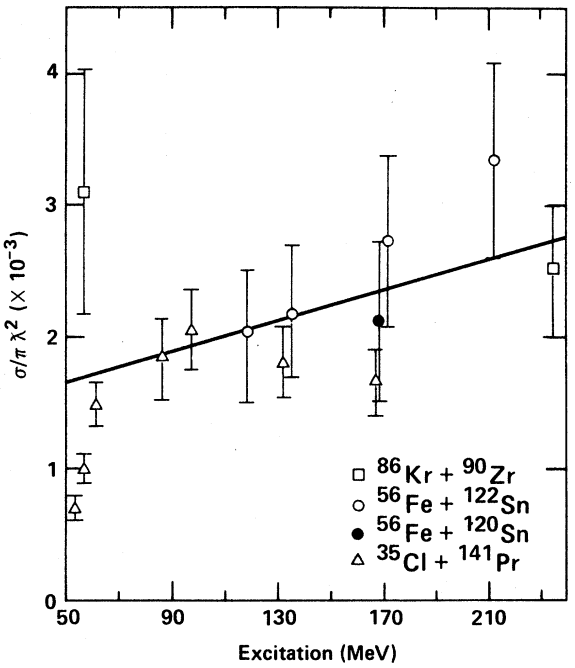

FIG. 6. Reduced ER cross sections versus excitation energy for three entrance channels to produce Os compound nuclei. The ER cross sections have been divided by $\pi\lambda^2$ of the entrance channels. Data sources are referenced in the text. The lowest energy Cl + Pr points do not fulfill the saturation requirement, and are shown to illustrate this point. An arbitrary line has been drawn to illustrate the correlation of the data versus excitation, supporting the saturation limit hypothesis.

lines selected are not unique. (In fact, the line in Fig. 6 resulted from a calculation which fitted the data as well as any arbitrary line, and so was retained for Fig. 6.) Certainly these data support the hypothesis that the σ_{ER} are limited by equilibrium fission competition. If so, they may be used for fitting by statistical models in order to deduce fission parameters, with no ambiguity due to other reaction mechanisms. For the Ar + Ag and Cl + Pr systems, some low energy points are shown which do not satisfy the saturation requirement ($\sigma_f \gg \sigma_{ER}$) in order to illustrate the difference in behavior.

Consider next the relationship of fusion trajectories of the three entrance channels ^{35}Cl+^{141}Pr, ^{56}Fe+^{122}Sn, and ^{86}Kr+^{90}Zr, in the context of the question of whether they should have similar or dissimilar entrance channel trajectories. These considerations are valuable in order to see if possible

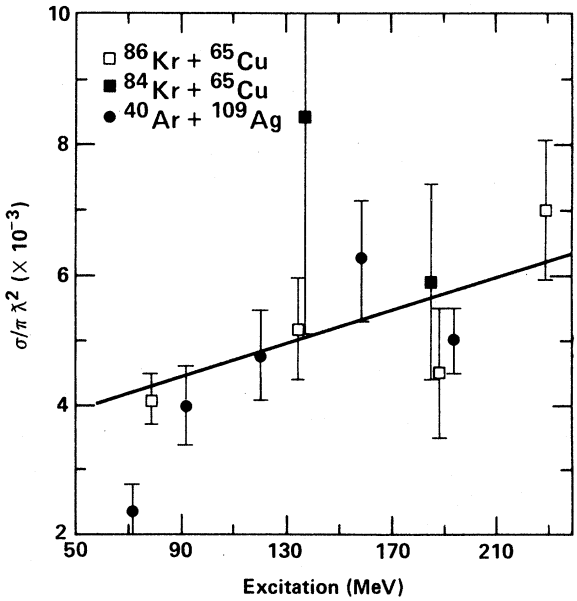

FIG. 7. As in Fig. 6, but for production of Tb compound nuclei. The lowest energy ^{40}Ar+^{109}Ag point does not satisfy the saturation requirement.

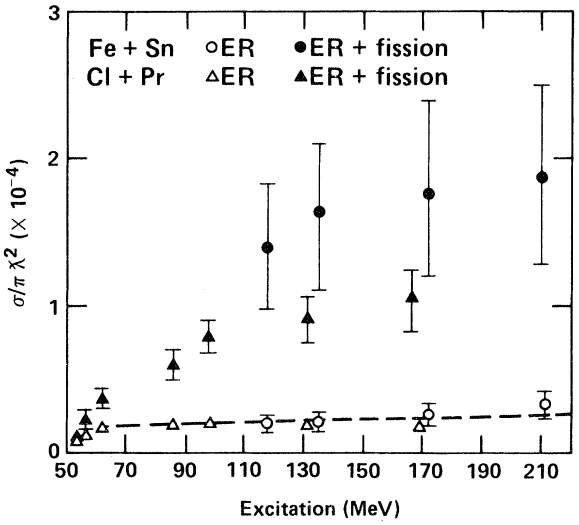

FIG. 8. Points shown as in Fig. 6, but also including results of reduced fusion cross sections ($\sigma_{ER}+\sigma$ fission-like). This illustrates the very expanded scales of Figs. 6 and 7, and puts into better perspective the good agreement of the reduced evaporation residue cross sections versus excitation. The low energy points for Cl + Pr illustrate the failure of the saturation condition ($\sigma_f > \sigma_{ER}$) to be satisfied.

systematic differences in the three target-projectile systems of Fig. 6 might indeed relate to the entrance channel rather than being due to experimental measurement. This can be done in a semiquantitative manner using the new dynamic model of Swiatecki,[13,14] in which a global scaling parametrization is employed. One point which can be treated fairly quantitatively is whether the contact configuration of the interacting ions can fuse unimpeded, or whether the configuration at contact is less compact than a conditional saddle point shape, thereby requiring an additional radial injection energy for fusion. In the context of Swiatecki's model, fusion means that the composite system will equilibrate in mass, charge, and excitation energy, but may not reach the true saddle point.

The position of the conditional saddle point is given by a numerical value of a disruptive parameter, very much in analogy with the critical fissility parameter for nuclear fission. The value which has mostly been used has been determined empirically by analyzing a large body of fusion data. The critical value of the disruptive parameter for the conditional saddle point was found to be ≈ 33.[14,15] Systems with a disruptive parameter less than this value should fuse unimpeded; systems with a greater disruptive parameter are impeded from fusion and require an extra radial injection energy to fuse; the parameter related to the slope of the extra radial injection energy has also been determined in this empirical fashion. These systems may have trajectories with very long time scales between the conditional and compound nucleus saddle points.

The disruptive parameter consists of two parts: Coulombic and centrifugal. The Coulombic parameter is defined using Bass's parameter,[16]

$$(Z^2/A)_{\text{Coul}} = 4Z_1Z_2/[A_1^{2/3}A_2^{2/3}(A_1^{1/3}+A_2^{1/3})] , \quad (1)$$

where Z_i (A_i) refer to target and projectile nuclear charge (mass).

The centrifugal scaling parameter is given as the square of the ratio of the entrance channel angular momentum to an angular momentum parameter J_{ch},

$$(Z^2/A)_{\text{cent}} = (J/J_{\text{ch}})^2 , \quad (2)$$

where

$$J_{\text{ch}} = \frac{e\sqrt{mr_0}A_1^{2/3}A_2^{2/3}(A_1^{1/3}+A_2^{1/3})}{2f(A_1+A_2)^{1/2}} , \quad (3)$$

where e is the proton charge, m is the nuclear mass unit, and $r_0 = 1.22$ fm. The symbol f represents the fraction of the total angular momentum responsible for the centrifugal force in the separation degree of freedom.

It is of interest to evaluate the total disruptive parameter for the systems shown in Fig. 6 first for the Coulombic contribution, and second for a value of the angular momentum for which the fission barrier B_f is approximately equal to the neutron binding energy B_n. It is in this range of angular momenta that fission is competing favorably with particle emission in determining the σ_{ER} survival cross section. Therefore, noncompound trajectories at higher values of J will not influence σ_{ER}, but noncompound trajectories below this value should begin to restrict or modify the σ_{ER} cross sections, as will be discussed.

For the three systems Cl + Pr, Fe + Sn, and Kr + Zr, Eq. (1) gives values of 27.9, 31.2, and 32.7, respectively (with the critical value being $\simeq 33$). Therefore, at zero angular momentum the Kr + Zr system at contact just reaches the conditional saddle point and is at the threshold of requiring an extra injection energy to fuse, whereas the Cl + Pr and Fe + Sn systems should fuse unimpeded. Computing the total disruptive parameters at $45\hbar$ ($B_f \simeq B_n$), assuming a value of f in Eq. (3) characteristic of rolling motion (which has been found to be consistent with a broad range of data),[9,14,15,17] gives

values of 30.4, 32.8, and 33.9, respectively. Here the Cl + Pr system can still fuse unimpeded, and Fe + Sn is at the threshold of requiring an extra injection energy, and may have slow trajectories between conditional and true saddle points. The Kr + Zr system is expected to require an extra injection energy for fusion.

The prediction by Swiatecki's model that these three entrance channels should have quite different fusion trajectories (in view of the great successes of this new dynamic model in reproducing a large body of experimental fusion data[17]) makes the comparisons in Fig. 6 particularly interesting. Unfortunately, the data are not of the quality which could be achieved with modern counters using an accelerator with higher beam quality and beam optics and in particular utilizing a recoil spectrometer. Evaporation residue results should be measurable to $\pm 5-7\%$ accuracy; results to $7-10\%$ have easily been attained using Van de Graaff accelerators. If the error bars of Fig. 6 could be reduced to the $5-7\%$ limit, then comparisons of this type could be extremely valuable concerning both precompound and postcompound particle evaporation. At this point we note only that the possible systematic discrepancies between different entrance channels in Fig. 6 are in the opposite direction to those expected for entrance channel effects.

Having shown that the saturation deexcitation requirement is in general satisfied by these data, we address the question of the sensitivity of such data to statistical fission parameters which would be determined in a model fitting procedure. This is the subject of Sec. V. We will not attempt to extract best parameters; this has been done in Ref. 19. Rather, we show that saturation ER data are sensitive to variations in statistical parameters and therefore valuable in their determination.

V. SENSITIVITY OF SATURATION DATA TO STATISTICAL PARAMETERS

A. Calculation options and parameters

It was shown in the previous section that the data of Figs. 6 and 7 support the hypothesis that the reduced cross sections are consistent with formation by decay of equilibrated systems (compound nuclei). In this section we test the sensitivity of the data to statistical parameter sets. The variables which we will test will be primarily the angular momentum dependent fission barriers $B_f(J)$ and the ratios of single particle level densities at saddle point to ground state, a_f/a_ν.

The calculations to be presented have been performed with the ALERT code[18]; this is a statistical Hauser-Feshbach code described in some detail in other works.[19,20] Relevant options are as follows.

1. Fission barriers. Angular momentum dependent fission barriers are based on the rotating liquid drop model (RLDM) of Cohen *et al.*[21] Options are programmed by which the barriers may be modified by three methods. They may be multiplied by a constant multiplier at all angular momenta. They may be modified by subtraction of a constant barrier decrement at all angular momenta [in this option the $B_f(J)$ resulting is a different fraction of the RLDM barrier at every value of J]. A third alternative is based on a scaling procedure using the finite range correction of Krappe, Sierk, and Nix for zero angular momentum systems.[22] The method used to scale their result with angular momentum has been discussed in detail in Ref. 19 and is not repeated here.

2. Single particle level density ratios. The level density routine computes level densities for every residual nuclide and for saddle points for each decaying nucleus defined by Z,A, and E,J. The a_f and a_ν values are computed for each nuclide at every J ($J=0$ to $J=100$) using the deformation dependence as given by Bishop *et al.*,[23] with deformations based on predictions of the RLDM.[21] Usually these results are used *a priori*; however, the a_f may all be scaled by an additional constant multiplier to provide flexibility in the a_f/a_ν ratio. The Bishop formula a_f and a_ν values were computed in this paper assuming $a=A/8$ for spherical nuclei.

3. Level density forms. The conventional form of the level density which assumes spherical symmetry will be used for results presented herein, both for residual nuclei with ground state deformation and for saddle point nuclei

$$\rho(U,J)=\frac{(2J+1)}{(8\pi\sigma^3)^{1/2}}\rho(U-U_{\text{yrast}})\ . \tag{4}$$

No shell effects are included, but pairing corrections are made. The option exists in the code to substitute level densities with collective enhancement.[24–26] Comparisons of the two approaches have been made in Ref. 19. We will mention the percentage change in σ_{ER} results which would result from collective enhancement, but not actually show these results. Evaluation of σ is discussed in Ref. 19; U_{yrast} is evaluated from RLDM.

4. Transmission coefficients for particle emission. The classical sharp cutoff algorithms described in Ref. 20 were used for generating n, p, and α

transmission coefficients. The option exists to do the calculation using T_l based on the RLDM predicted deformations of the residual nuclei. This option was not exercised for most results presented in this work. Comparisons between the two options were presented in Ref. 19, and differences for the systems in Fig. 6 resulting from these options will be mentioned. The ALERT code is limited to excitation energies of ≤ 200 MeV; results of calculations presented beyond this limit represent extrapolations.

B. Comparisons of calculated and experimental reduced cross sections

In Figs. 9 and 10, we present results of statistical calculations compared with the data previously summarized in Figs. 6 and 7. The calculated result shown by the solid lines represents the $a_f(J)$ and $a_\nu(J)$ results of RLDM (Ref. 21) and the Bishop formula,[23] which leads approximately to an a_f/a_ν ratio of 1.02 for $A=149$ and 1.03 for $A=176$. The

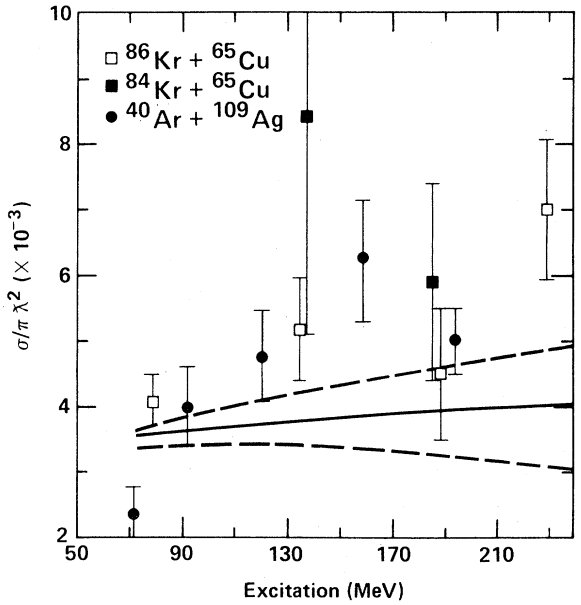

FIG. 10. As in Fig. 9 for the Tb compound nucleus system.

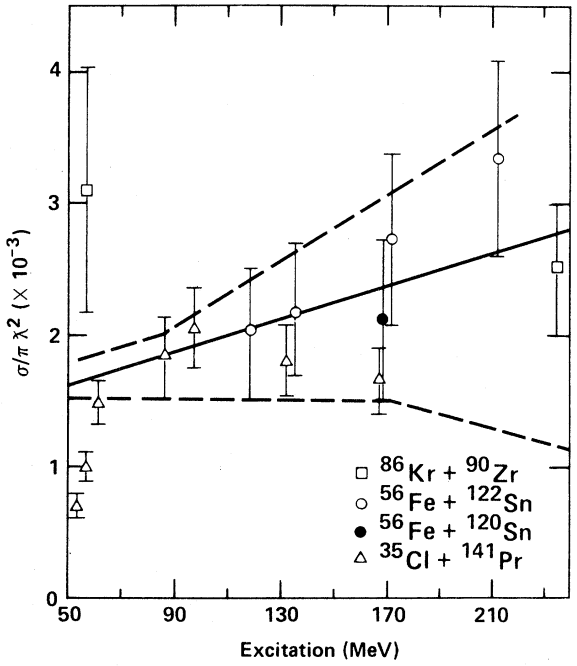

FIG. 9. Data as in Fig. 6 compared with results of statistical model calculations. The solid line represents the $a_f(J)/a_\nu(J)$ calculated according to Bishop *et al.*, with RLDM barriers reduced with scaled finite range correction as described in Ref. 19. The upper dashed curve is changed only in that $a_f(J)$ was multiplied by 0.98; for the lower dashed curve $a_f(J)$ was multiplied by 1.02. All calculated results above 200 MeV excitation have been extrapolated.

dashed curves above the solid curves differ only in that all $a_f(J)$ were multiplied by 0.98 (i.e., yielding $a_f/a_\nu \simeq 1.00$ for $A=149$ and $a_f/a_\nu \simeq 1.01$ for $A=176$). In the lower dashed curves the $a_f(J)$ were increased by 1.02 (i.e., $a_f/a_\nu \simeq 1.04$ for $A=149$ and 1.05 for $A=176$). Calculations were done wherever experimental points are indicated, and connected by straight line segments, giving the apparent abrupt slope changes for some of the calculated results. The fission barriers were given by the RLDM with correction at each J by the angular momentum dependent finite range scaling discussed in Ref. 19. These barrier results are shown in Fig. 11 for reference.

Figures 9 and 10 show that "fitting" of the reduced cross sections (RCS) is extremely sensitive to small variations in a_f/a_ν, and that the sensitivity increases with increasing mass. Changes in a_f/a_ν affect the *slope* of the RCS curve, as well as the distribution of first chance versus higher chance fission; i.e., as a_f/a_ν decreases, the fraction of multiple chance fission increases—and as a result more of the initial population survives fission, and the positive slope of the RCS versus excitation curve increases.

Sensitivity to fission barrier height adjustment is shown in Figs. 12 and 13. For the solid curves, the RLDM fission barriers were used without modification, whereas in the lower curves $B_f(J)$ were RLDM values reduced by 3 MeV. The $a_f(J)$ and

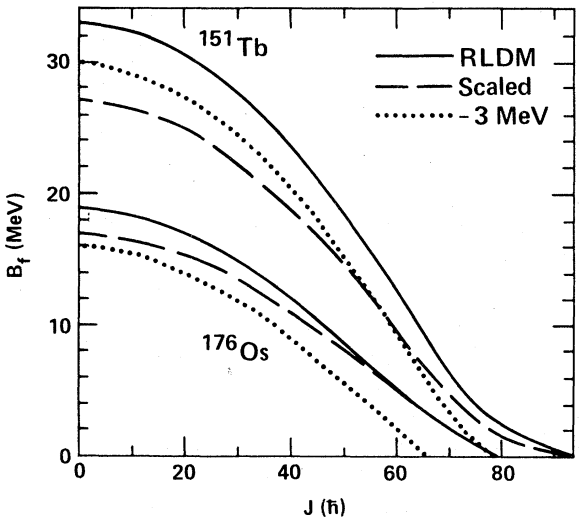

FIG. 11. Angular momentum dependent fission barriers for ^{151}Tb and ^{176}Os nuclei from RLDM, RLDM with finite range scaling correction, and RLDM decremented by 3 MeV at every value of J.

$a_\nu(J)$ are the same used for the solid lines of Figs. 9 and 10. It may be seen that barrier height adjustments tend to give parallel sets of curves, whereas a_f/a_ν adjustments tend to be reflected in changes

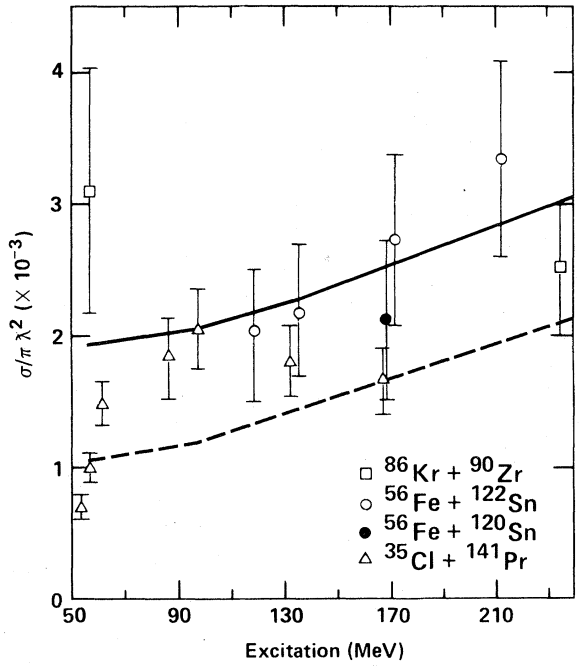

FIG. 12. Data as in Fig. 6 compared with statistical model calculations using RLDM barriers without modification (upper curve) and reduced by 3 MeV at every value of J (lower curve). The $a_f(J)/a_\nu(J)$ were based on the RLDM shapes and Bishop formula as discussed in Ref. 19.

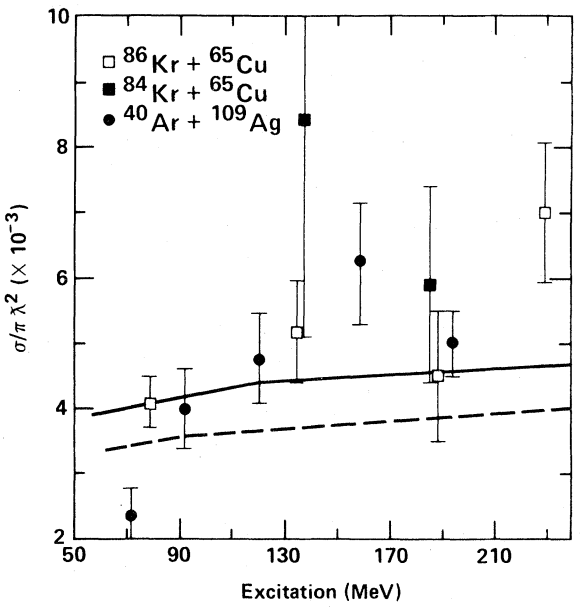

FIG. 13. As in Fig. 12 for the Tb compound nucleus system.

of slope in the RCS representation. This suggests that data of higher quality in the saturation region may permit quite precise determination of both ΔB_f and a_f/a_ν. A difference of 3 MeV in $B_f(J)$ makes an appreciable change in the predicted RCS results for $A=176$, and a significant change for $A=149$. A best result could be selected to within $a\pm1$ MeV uncertainty in the $A=176$ region, which is as well as could be done in the $\sigma_f \ll \sigma_{ER}$ region fitted in Ref. 19. Sensitivity (for good data) would be nearer ±1.5 MeV at $A=149$. If the level density option for collective enhancement is used in these calculations, the σ_{ER} predicted for the $A=176$ system decrease by approximately 10%. This is a much lesser amount than is found for the nonsaturation region, where changes (and therefore uncertainties) of 30–50% were found. Similarly, the sensitivity to using T_l modelled for deformed nuclei is less in the saturation region than in the lower energy region, although we feel that this option should be exercised when attempting to extract fission parameters from a data set. Use of T_l for deformed nuclei in these systems resulted in changes of $\lesssim 2\%$ in σ_{ER}, whereas σ_f in Ref. 19 showed up to 300% changes in going from deformed nucleus T_l to spherical nucleus T_l values.

The statistical model calculations of this work have been performed assuming compound nuclei populated for all partial waves from 0 to $80\hbar$. Some calculations were also repeated for compound nuclei in the range 0 to $70\hbar$ and 0 to $100\hbar$. The re-

sulting σ_{ER} were unchanged, as expected—and as must be the case if the saturation condition is fulfilled. The parameters of Fig. 12 are in good agreement with results of Ref. 19, while those of Fig. 13 are not consistent, and remeasurement of several experimental results would be valuable in order to understand reasons for the discrepancies.

VI. CONCLUSIONS

We have shown that ER excitation functions measured in the fission saturation region can provide valuable data for determination of statistical fission parameters. Data of this type may offer some very strong advantages over data in the region for which $\sigma_f \ll \sigma_{ER}$.

First, it is only necessary to measure σ_{ER} accurately (whereas σ_{ER} and σ_f must both be measured to high accuracy in the nonsaturation region). With the advent of on-line recoil spectrometers to separate Rutherford scattered projectiles from ER products at small angles, it should be possible to measure σ_{ER} to quite a high accuracy. If additionally a cross bombardment of the type illustrated in, e.g., Fig. 6, is made, it is possible to test to see if the data satisfy the Bohr hypothesis by illustrating that the reduced cross sections depend only upon excitation energy. In contrast, for nonsaturated systems one must have some knowledge of cutoff of high spin populations for each entrance channel and bombarding energy. Therefore a simple model independent Bohr test such as in Fig. 6 is not possible in the nonsaturation systems.

In the saturation systems the entrance channel partial wave at which $B_f = B_n$ (somewhat beyond which the saturation condition is achieved) may be a quite central collision (in that the reaction cross section may extend easily beyond $100\hbar$ in heavy ion reactions). If so, then partial fusion/direct reactions may reasonably be expected to set in at partial waves considerably beyond those of relevance in determining saturation ER yields.

For systems for which $\sigma_f \ll \sigma_{ER} \simeq \sigma_{fusion}$, fusion may cease to take place because some fraction of higher partial waves begin to go into noncompound fusion or direct reactions. It is some small fraction of partial waves in this region, in competition with noncompound reactions, which are likely to make up the fission cross section.[27–30] Because the fission to total width ratio may be exponentially increasing with angular momentum in this region, statistical parameters extracted from data analysis may be very sensitive, e.g., to the assumption of the width of the angular momentum cutoff between compound and noncompound reactions. One may find different statistical parameters resulting if a classical sharp cutoff is assumed versus a diffuse cutoff. In general this ambiguity will be worse as σ_f/σ_{ER} gets smaller.

The nonsaturation data on the other hand can also offer information of a type not accessible by saturation analyses, and so the two regions should be viewed as complementary in tackling the very difficult question of angular momentum dependent fission barriers. These data always allow one to probe lower angular momenta than the saturation data, and will permit testing of statistical parameters over only a few partial waves, and often with less of a contribution from multiple chance fission than for the saturation data. The saturation data are restricted in sensitivity to a range of partial waves approximately in the $B_f \simeq B_n$ region, and when σ_{ER} is a small fraction of the fusion cross sections. The saturation data tend to be far less sensitive to parameter variations than the nonsaturation data.

From the arguments above we conclude that the saturation and nonsaturation data are complementary to the problem of mapping out statistical fission parameters at high angular momenta; each should be used, and the uncertainties of the results estimated taking into consideration the intrinsic weakness of each data set.

It has been suggested that statistical fission parameters extracted from data of the type presented here, and also in the nonsaturation region, are so physically unrealistic that they must indeed result from invalid analyses of noncompound reaction products.[31,32] Yet the Bohr independence hypothesis comparisons of this work confirm that the products are consistent with formation by equilibrium decay processes. Comparisons of fission parameters extracted from these and other data with the finite range model predictions[19] gives quite reasonable agreement. The comparisons of this work and the parameters of Ref. 19 seem to suggest that the statistical parameters deduced are both physically meaningful and reasonable. They further show no basic incompatibility between parameters deduced from experiments due to different groups and spanning a broad compound nucleus mass range.

This work was performed under the auspices of the U.S. Department of Energy by the Lawrence Livermore Laboratory under Contract number W-7405-ENG-48.

[1]J. R. Huizenga, R. Chaudhry, and R. Vandenbosch, Phys. Rev. 126, 210 (1962).
[2]J. Bisplinghoff *et al.*, Phys. Rev. C 17, 177 (1978); P. David *et al.*, Nucl. Phys. A287, 179 (1977).
[3]M. Beckerman and M. Blann, Phys. Rev. C 17, 1615 (1978), and references therein.
[4]H. C. Britt *et al.*, Phys. Rev. C 13, 1483 (1976).
[5]F. Plasil *et al.*, Phys. Rev. Lett. 45, 333 (1980).
[6]W. von Oertzen *et al.*, Z. Phys. A 298, 207 (1980).
[7]D. J. Hinde, thesis, Australian National University, Canberra, Australia, 1982 (unpublished).
[8]H. Karwowski, thesis, Indiana University, 1980 (unpublished).
[9]B. Sikora *et al.*, Phys. Rev. C 25, 686 (1982).
[10]B. Sikora *et al.*, Phys. Rev. C 25, 1446 (1982).
[11]F. Plasil *et al.*, Phys. Rev. C 18, 2603 (1978).
[12]H. H. Gutbrod, W. G. Winn, and M. Blann, Nucl. Phys. A213, 267 (1973).
[13]W. J. Swiatecki, Phys. Scr. 24, 113 (1981).
[14]W. J. Swiatecki, Nucl. Phys. A376, 275 (1982).
[15]H. Sann *et al.*, Phys. Rev. Lett. 47, 1248 (1981).
[16]R. Bass, Nucl. Phys. A231, 45 (1974).
[17]M. Blann and D. Akers, Phys. Rev. C 26, 465 (1982).
[18]M. Blann and T. Komoto, University of California Radiation Laboratory Report UCID 19390, 1982 (unpublished).
[19]M. Blann and T. Komoto, Phys. Rev. C 26, 472 (1982).
[20]M. Blann and T. Komoto, Phys. Rev. C 24, 426 (1981).
[21]S. Cohen, F. Plasil, and W. J. Swiatecki, Ann. Phys. (N.Y.) 82, 557 (1974).
[22]H. J. Krappe, A. J. Sierk, and J. R. Nix, Phys. Rev. 20, 992 (1979).
[23]C. J. Bishop, I. Halpern, R. W. Shaw, Jr., and R. Vandenbosch, Nucl. Phys. A193, 161 (1972).
[24]T. Ericson, Nucl. Phys. 6, 62 (1958).
[25]H. Freiesleben, H. C. Britt, and J. R. Huizenga, in *Proceedings of the Third International Atomic Energy Symposium on Physics and Chemistry of Fission 1973* (International Atomic Energy Agency, Vienna, 1974), Vol. I, p. 447.
[26]S. Bjornholm, A. Bohr, and B. R. Mottelson, in *Proceedings of the Third International Atomic Energy Symposium on Physics and Chemistry of Fission 1973* (International Atomic Energy Agency, Vienna, 1974), Vol. I, p. 373.
[27]R. Bimbot, D. Gardes, and M. F. Rivet, Nucl. Phys. A189, 193 (1972).
[28]K. Siwek-Wilczynska *et al.*, Phys. Rev. Lett. 42, 1599 (1979).
[29]P. D. Croft and J. M. Alexander, Phys. Rev. 165, 1380 (1968).
[30]K. A. Geoffroy *et al.*, Phys. Rev. Lett. 43, 1303 (1979).
[31]G. J. Mathews and L. G. Moretto, Phys. Lett. 87B, 331 (1979).
[32]L. G. Moretto, in *Nuclear Structure and Heavy Ion Collisions Proceedings for the International School of Physics Enrico Fermi, Course XL, 1981,* edited by R. A. Broglia and R. A. Ricci (North-Holland, Amsterdam, 1981), p. 41.